

FLOW PROCESSES AND SEDIMENTATION IN A LOW-SINUOSITY HIGH
NET-SAND CONTENT FLUVIAL CHANNEL BELT: 3D OUTCROP STUDY
OF THE CEDAR MOUNTAIN FORMATION, UTAH

by

Bradley Nuse

A thesis submitted to the Faculty and the Board of Trustees of the Colorado School of Mines in partial fulfillment of the requirements for the degree of Master of Science (Geology).

Golden, Colorado

Date _____

Signed: _____
Bradley R. Nuse

Signed: _____
Dr. David R. Pyles
Thesis Advisor

Signed: _____
Dr. John Humphrey
Thesis Advisor

Golden, Colorado

Date _____

Signed: _____
Dr. Paul Santi
Professor and Head
Department of Geophysics

ABSTRACT

This thesis documents the locations and proportions of lithofacies, morphometric characteristics and continuity of sandstone of a 3D exposure of an ancient fluvial channel belt in the Cedar Mountain Formation. Morphometric measurements include: width (80m), thickness (6.3 m), sinuosity (1.2), radius of curvature (right: 175 m, left: 220 m) bend curvature (right: 2.2, left: 2.8), and aspect ratio (12.7). Additionally, using cross-cutting relations, superposition, and facies type, the sequential evolution of the channel belt is interpreted. Using photopanels and measured sections, three primary lithofacies are documented. Facies within the channel belt are cross-stratified sandstone, conglomerate, and ripple-to-planar laminated sandstone. Lithofacies are quantified by geomorphic position (outside bend, inside bend, and inflection point) in the studied channel belt. Sandstone is continuous across the entire outcrop, however, bedsets and stories do not longitudinally persist the entire wavelength of the channel belt. Furthermore, we interpret that high-energy flows incised into the adjacent mudstone to create channel for fluid and sediment to flow through. Next, a high-energy conglomerate was deposited across the base of the channel as it began to migrate laterally although conglomerate is thickest at inflection points. Finally, using superposition and low-flow regime structures, we interpret that laterally accreting and downstream accreting bars filled the channel belt to the point of avulsion. These results can be used to update previous fluvial reservoir models to predict the spatial location and proportions of lithofacies within a reservoir. Updated reservoir model helps predict flow units and preferential fluid migration pathways in the subsurface.

TABLE OF CONTENTS

ABSTRACT.....	iii
LIST OF FIGURES	v
LIST OF TABLES	vi
ACKNOWLEDGMENTS	vii
CHAPTER 1 INTRODUCTION	1
CHAPTER 2 GEOLOGICAL SETTING.....	7
CHAPTER 3 DATA & METHODOLOGY	11
3.1 Fluvial Hierarchy	12
3.2 Lithofacies	13
CHAPTER 4 RESULTS	19
CHAPTER 5 DISCUSSION	23
5.1 Continuity and Applications	23
5.2 Sequential Evolution and Flow Processes.....	25
CHAPTER 6 CONCLUSIONS	30
REFERENCES CITED	31
APPENDIX A Measured Sections and Cross Sections	36
APPENDIX B Outcrop Photopanel.....	37

LIST OF FIGURES

Figure 1.1	End-member styles for sandstone distributions in fluvial channel fill.....	4
Figure 1.2	Hierarchical classification scheme	5
Figure 1.3	Oblique aerial photograph of the field area	6
Figure 2.1	Study location map	9
Figure 2.2	Geologic map of study area	10
Figure 3.1	Dip-oriented and strike-oriented cross-sections	14
Figure 3.2	Paleocurrent plots and rose diagram	15
Figure 3.3	Representative photopanel of Channel Belt A, Segment 4	16
Figure 3.4	Photographic examples of lithofacies.....	17
Figure 4.1	Lithofacies proportions at different geomorphic locations	21
Figure 4.2	Thickness and lithofacies contour maps	22
Figure 5.1	Schematic evolution of Channel Belt A	29

LIST OF TABLES

Table 3.1	Morphometric characteristics of Channel Belt A, Segment 4	17
Table 3.2	Description of lithofacies	18

ACKNOWLEDGMENTS

There are many people whom have made this project possible. The continual support and motivation of my family and close friends, was constantly given and was greatly appreciated. Without it, the process would have been much, much harder.

I would to thank all my field assistants Marty Droze, Andrew Shaw, Peter Brice, and Lauren Cross, who gave their precious time to make ensure my safety, help me think through problems, and keep me company in my field area. I want to express extreme gratitude to my CoRE team for technical, geological, and emotional support throughout this project: Jane Stammer, Jeremiah Moody, Jesse Pisel, Greg Gordon, Kimber O'Brien, Matt Andreson, Cathy Van Tassel, Mark Kirschbaum and David Pyles.

I am extremely grateful to Mark Kirschbaum and Jesse Pisel. The knowledge and help received from both was invaluable and crucial to completing the entire project. Both answered countless questions and helped during the entire project from start to finish.

Finally, I am particularly grateful to my advisor Dr. David Pyles. The knowledge, enthusiasm, and criticism made me a better geologist and scientist. The quality of this project could have not been achieved without the help of Dr. Pyles.

The funding for this research was provided by the Chevron Center of Research Excellence.

CHAPTER 1

INTRODUCTION

Fluvial channels and their associated deposits represent one of the most extensive depositional environments on earth (Qui et al., 1987). To aid fluvial reservoir modeling, previous studies have focused on fluvial facies, fluvial reservoir modeling, and fluvial architecture analysis (e.g. Galloway et al., 1982; Collinson and Lewin, 1983; Schumm, 1985; Qiu et al., 1987; Kerr and Jirik, 1990; Miall and Tyler, 1991; Doyle and Sweet, 1995; Bridge, 2006; Miall, 2006; Slatt, 2006; Fielding et al., 2009; Ghazi and Mountney, 2009; Colombera et al., 2012a, b). The quantitative description of sand-prone systems is important because it provides: 1) an improved understanding of the fundamental nature of sand-prone systems (stacking patterns, volumetrics, etc.), and 2) the application of data to modeling depositional characteristics of such systems, such as basin analysis and reservoir modeling (Drinkwater and Pickering, 2001).

The producibility of fluvial reservoirs is a function of sandstone connectivity and continuity (Larue and Hovadik, 2006). In this context, connectivity refers to the interconnectedness of sandstones between stratigraphically adjacent channel belts, whereas continuity refers to the longitudinal and lateral persistence of sandstones within fluvial channel belts (Larue and Hovadik, 2006). In other words, connectivity refers to how channel belts are connected to one another and continuity refers to how internal features of channel belts, such as barforms, are connected to one another. There are two alternative models regarding reservoir connectivity. First, Larue and Friedmann (2005) and Larue and Hovadik (2006) created reservoir models of fluvial channel systems, whereby the degree of amalgamation between stratigraphically adjacent

channel belts was varied from little to high degree of amalgamation. Critically, the channel belts were modeled as continuous belts of sandstone, with no internal heterogeneity, similar to that depicted in Figure 1.1A. Larue and Friedmann (2005) and Larue and Hovadik (2006) document that even when a small amount of amalgamation exists between stratigraphically adjacent channel belts, the reservoir and associated sandstones are fully connected. Second, Pranter et al. (2007 and 2008) conducted a similar study in which sandstone in channel belts were modeled as having low continuity, similar to the channel belt depicted in Figure 1.1B, in which sandstones are only located in point bars of channel belts. Pranter et al. (2007 and 2008) determined that channel belts are highly heterogeneous and not well connected due to intrachannel mudstone that separated lateral accretion packages. It is evident from these studies that intra-channel continuity is a key driver for connectivity.

Few studies have focused on intra-channel continuity, the most notable example is Donselaar and Overeem (2008). Donselaar and Overeem's (2008) research was based on a hypothesis that intra-channel continuity is dictated by the types of bars (downstream vs laterally accretings) that fill the fluvial channel belts (Figure 1.1). Ford and Pyles (2014) proposed two end-member fill styles for fluvial channel belts (Figure 1.2): 1) those filled primarily by lateral accretion deposits; and 2) those filled primarily by downstream accretion deposits. Channel belts containing primarily downstream accretion deposits are interpreted to contain higher sandstone continuity than their laterally accreting counterparts (Donselaar and Overeem, 2008). This thesis is focused on the latter model of a channel belt that is filled with a downstream-accreting fill.

The goal of this research is to improve our understanding of longitudinal continuity, sequential evolution, and sedimentation style in a low-sinuosity channel belt that contains both downstream accretion deposits and lateral accretion deposits (similar to Figure 1.1A).

A three-dimensional exposure of a fluvial channel belt in the Cedar Mountain Formation is the focus of this study (Figure 1.3). The Cedar Mountain Formation is ideal because it contains multiple channel belts that are exposed as sinuous ridges that persist across the landscape (Young, 1960; Stokes, 1961; Derr, 1974; Harris, 1980; Williams et al., 2007) making this a world class outcrop to address the goals of this study.

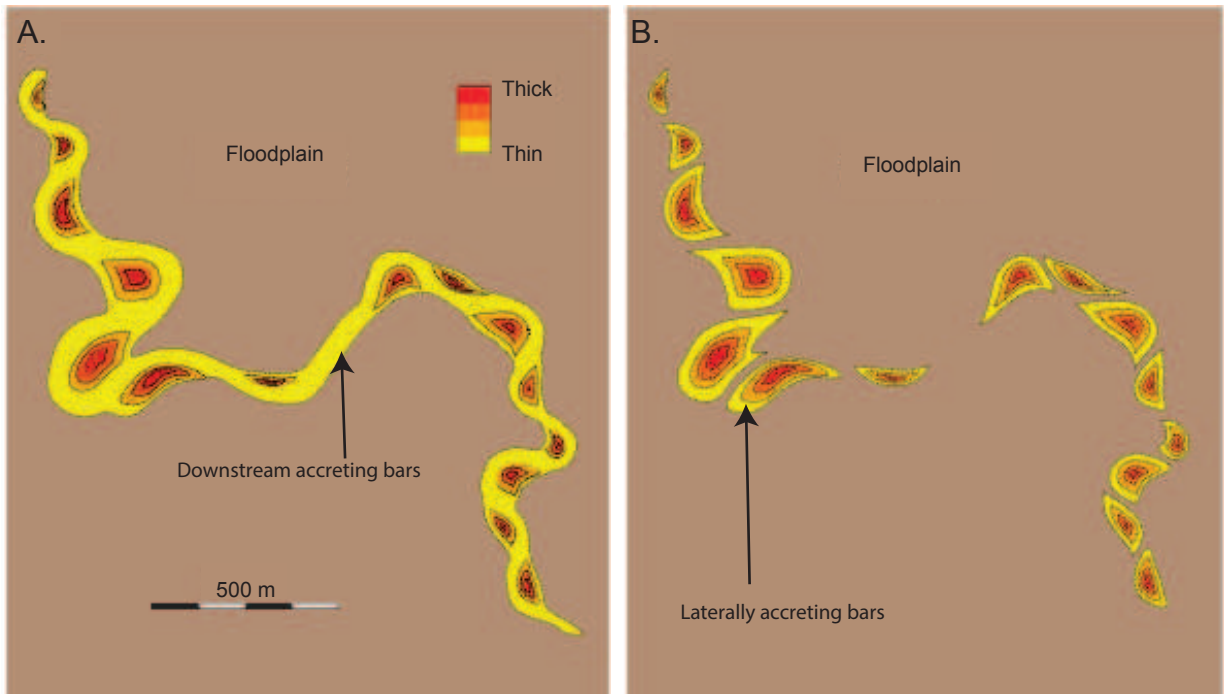


Figure 1.1: Diagrams depicting end-member styles for sandstone distributions in fluvial channel belts (from Donselaar & Overeem, 2008). A) Sandstone is located in point bars and in the channel fill forming a spatially interconnected network of sandstone. B) Sandstone is only located in the point bars, forming a number of spatially isolated volumes of sandstone.

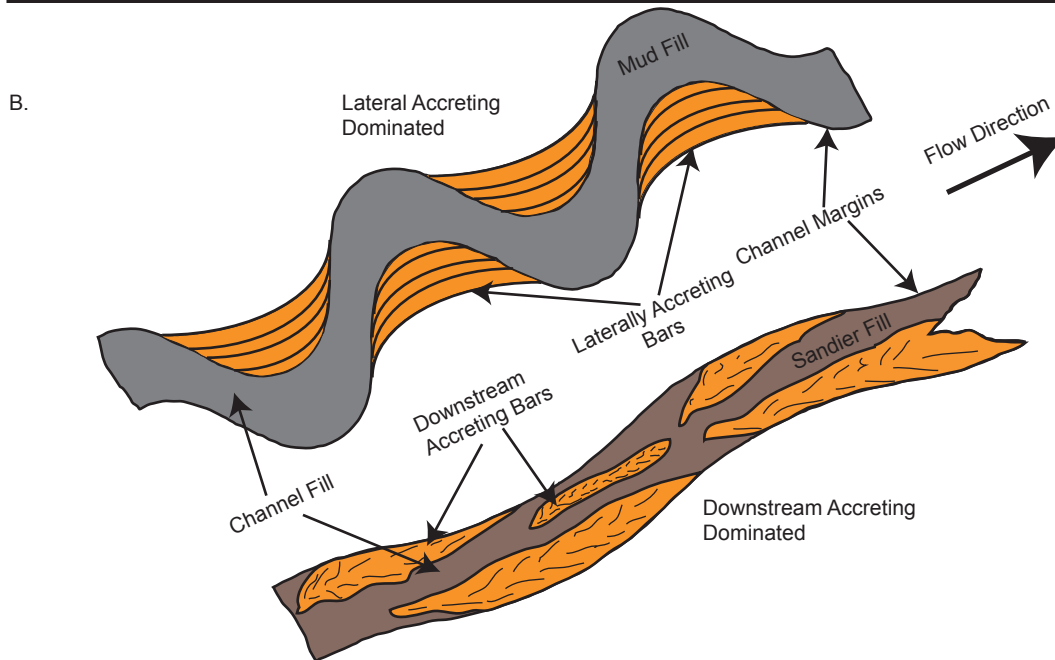
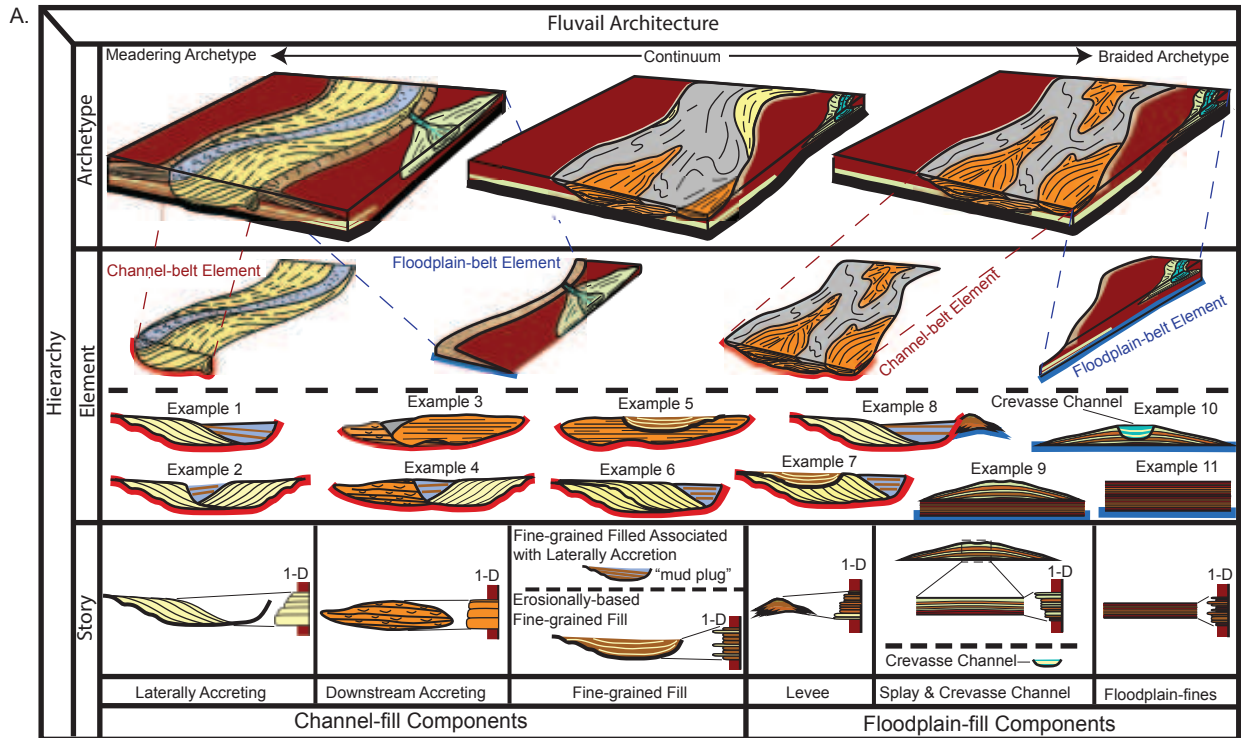


Figure 1.2: A) Schematic diagram of methodology developed by Ford and Pyles (2014) for fluvial hierarchy of architectural elements. Time span of deposition, cross-cutting relationships, and superposition increase in an upward transect through the hierarchical levels. Figure components are not drawn to scale. B) Diagrams depicting end-member classes of fluvial channels based on the intra-channel bar migration (from Ford and Pyles, 2014): (Upper) Channel belts containing predominantly laterally accreting bars, and (Lower) channel belts containing predominantly downstream accreting bars.

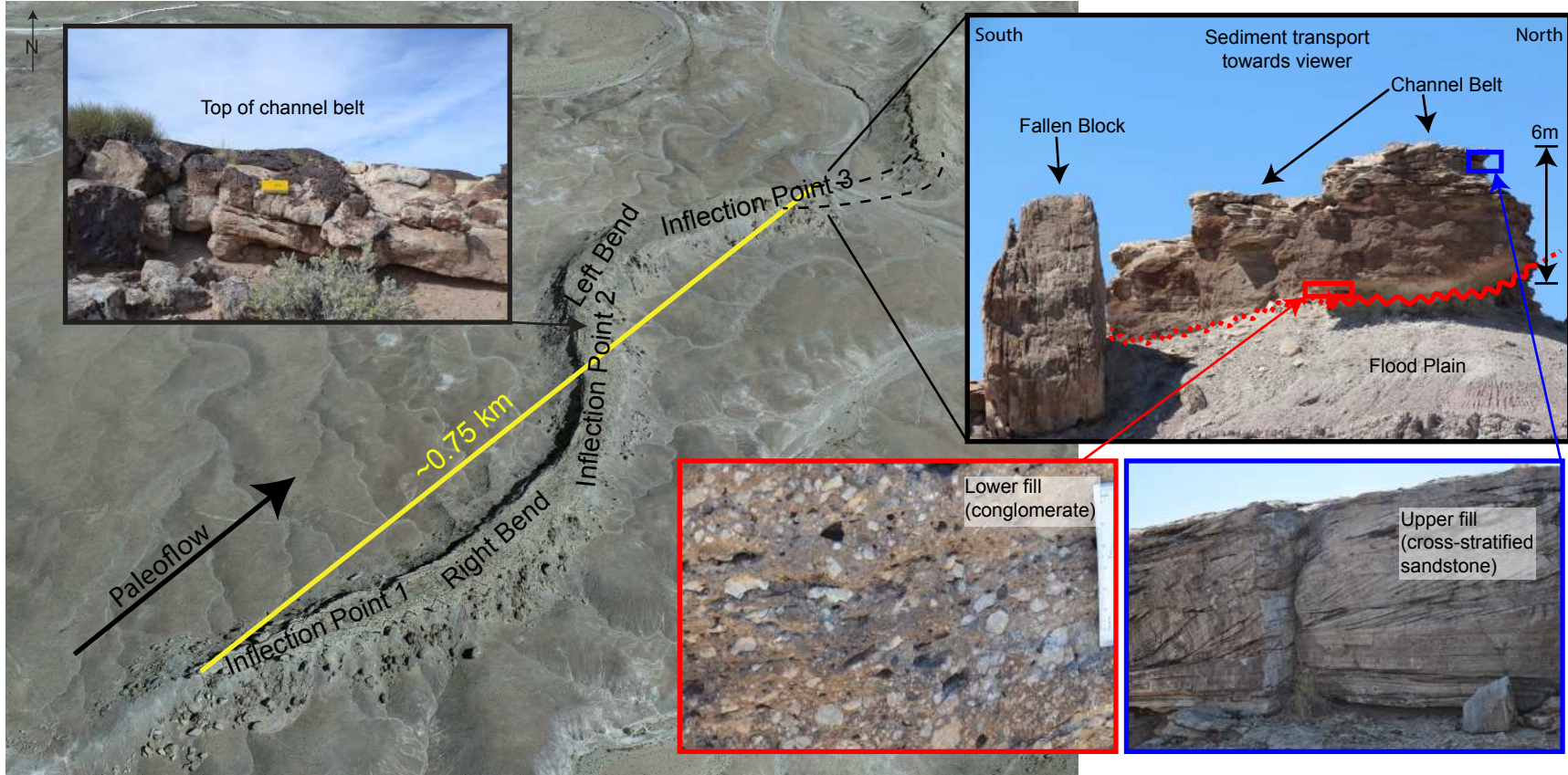


Figure 1.3: Oblique aerial photograph (from Google Earth) documenting the geomorphic expression of the studied channel-belt segment. Inset photographs (right) show the upward succession of facies. This study is focused on a ~1 km long segment of a fluvial channel belt in which two channel bends are exposed and the channel belt forms an elongate ridge. Location shown in Figure 2.1.

CHAPTER 2

GEOLOGICAL SETTING

The Lower Cretaceous (Aptian-Albian), fluvial Cedar Mountain Formation crops out in central Utah, east of the San Rafael uplift (Kirkwood, 1976; Currie, 1998; Williams et al, 2011). The field area is located approximately 15 kilometers southwest of the town of Green River, Utah (Figure 2.1).

The Cedar Mountain Formation unconformably overlies the Jurassic Morrison Formation and unconformably underlies the Cretaceous Dakota Sandstone, which is in turn overlain by the Mancos Shale (Figure 2.2). The Cedar Mountain Formation is subdivided into the Buckhorn Conglomerate and overlying Ruby Ranch Member (Figure 2.2B) in the study area (Harris, 1980; Williams et al., 2007). The basal Buckhorn Conglomerate crops out to the west and east of the study area as a matrix-supported pebble conglomerate that, in general, fines upward from pebbles and cobbles to medium-grained sand. The clasts are composed of chert, quartzite, and other clastic material. The Ruby Ranch Member contains lenticular conglomeratic sandstones with predominantly northeastward paleocurrents that crop out as elongate ridges in the area (Figures 1.3, 2.2). The adjacent mudstones contain abundant limestone nodules and are interpreted as the associated floodplain deposits (Kirkwood, 1976; Harris, 1980; Currie, 1998; Lorenz et al., 2006).

The Cedar Mountain Formation was deposited in a foreland basin that was located basinward of the Sevier Highlands (DeCelles et al., 1995; DeCelles and Currie, 1996; DeCelles and Giles, 1996). The subsequent deposition of the Dakota Sandstone and Mancos Shale buried the Cedar Mountain Formation. Erosion related to the uplift

of the Colorado Plateau exposed the paleochannels in the Cedar Mountain Formation as elongate ridges (Stokes, 1944; Harris, 1980; DeCelles et al, 1995; DeCelles and Currie, 1996; DeCelles and Giles, 1996; Williams et al., 2011). Williams et al. (2011) referred to the elongate outcrops of fluvial channels as “inverted topography” because the once entrenched channels now form ridges on the surface.

The basal Buckhorn Conglomerate is interpreted as a braided-river deposit (Harris, 1980). Harris (1980) interpreted that clasts within the conglomerate in the fluvial channels of the Cedar Mountain Formation are derived from the near-by Sevier highlands and the underlying Brushy Basin Member of the Morrison Formation. Harris (1980) interpreted the Ruby Ranch Member to contain alluvial plain deposits, shallow lake deposits, and stable, non-migrating, fluvial channel belts. Channel Belts A, B, C, D, and E all crop out as sinuous ridges that can be observed in three-dimensions (Figure 2.2). However, Channel Belt A, specifically Segments 4 and 5, has the best exposure of all the channel belts in the area. Therefore the main focus of this study is on Segments 4 and 5 of Channel Belt A of the Ruby Ranch Member (Figures 1.3, 2.2A), because the sedimentary structures are exceptionally well exposed (Figure 1.3) and morphometric characteristics can be measured, and stratigraphic surfaces are particularly well exposed. Segment 4 exposes 2 bends in the channel belt whereas Segment 5 exposes a strike-view cross section of the channel belt and its adjacent floodplain deposits (Figure 1.3). Note that the lateral margins have eroded away but a perfect cross-section is exposed in Segment 5. The channel-belt fill generally fines upward from very-coarse grained sands to fine grained sands (Figure 1.3) (Harris, 1980; Currie, 1998).

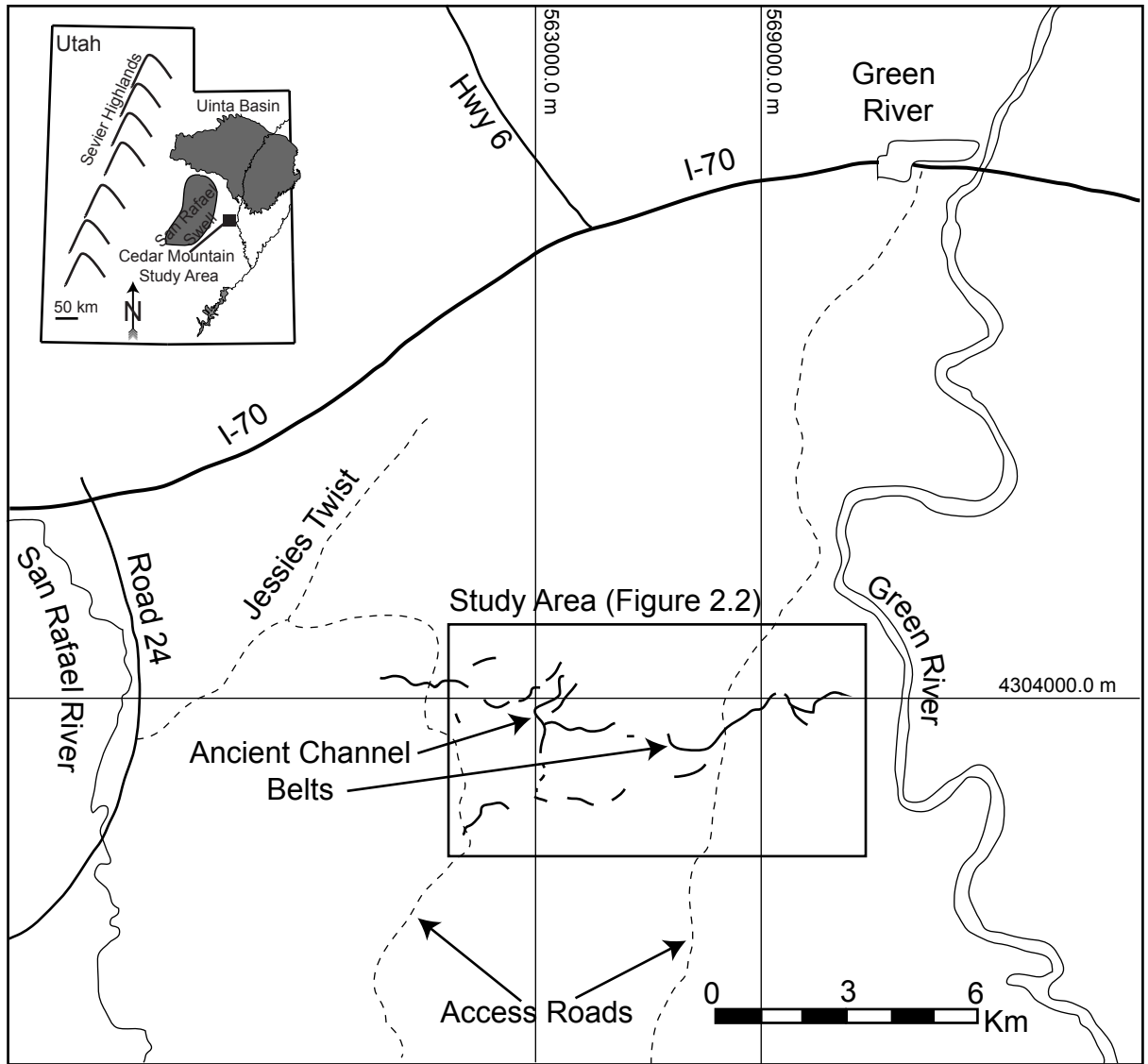
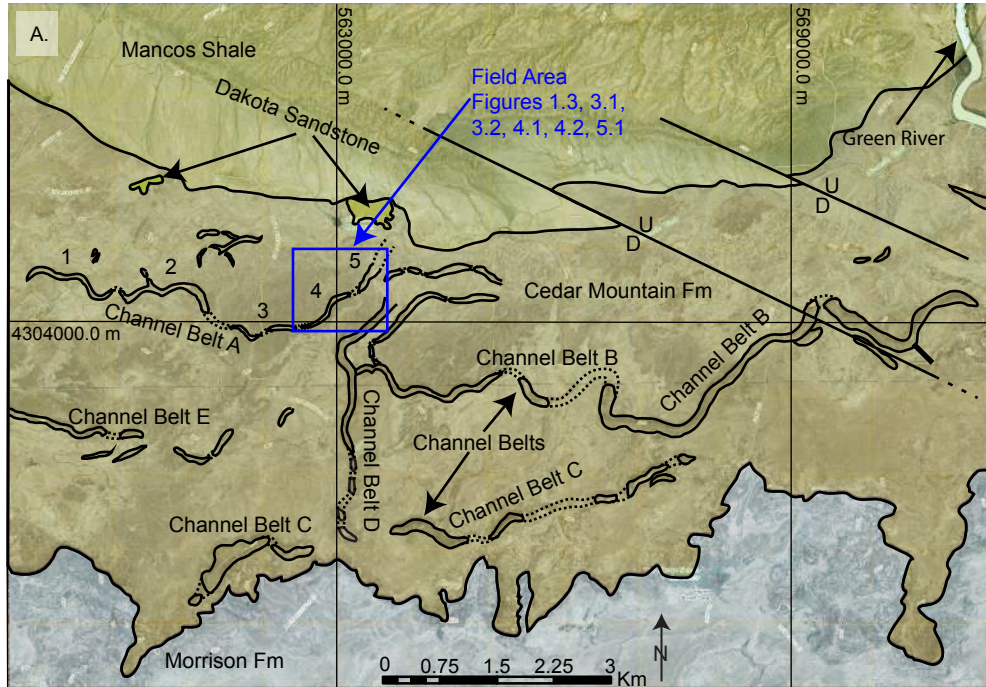


Figure 2.1: Location map of study area (UTM Zone 12S) (Modified from Harris, 1980).



B.

AGE	MAP UNIT	MAP UNIT		Schematic Column	
		Feet	Meters		
LATE CRETACEOUS (99-65 Ma)	Mancos Shale		3000	900	[Schematic Column]
		Ferron Ss Mbr	10-30	3-9	
		Tununk Mbr	350-400	110-120	
		Dakota Ss	0-30	0-9	
EARLY CRETACEOUS (145-99 Ma)	Cedar Mtn Fm	Ruby Ranch Mbr	60-90	20-30	[Schematic Column]
		Buckhorn Cngl Mbr	20-30	6-9	
LATE JURASSIC (161-145 Ma)	Morrison Fm	Brushy Basin Mbr	240-420	70-130	[Schematic Column]
		Salt Wash Mbr	160-290	50-90	
		Tidwell Mbr	20-50	6-15	

Figure 2.2: A) Geologic map documenting the boundaries of the Cedar Mountain Formation and stratigraphically adjacent units. The ribbon shaped units in the Cedar Mountain Formation are elongate ridges that are ancient channel belts (labeled as channel belts A-E). This study is focused on segments 4 and 5 of Channel Belt A (Map modified from Harris, 1980). Location shown in Figure 2.1. B) Stratigraphic chart of Late Jurassic to Late Cretaceous strata in central Utah showing the stratigraphic position of the Cedar Mountain Formation (Chart modified from Williams et al., 2007). Note: Colors on chart match those on map.

CHAPTER 3

DATA AND METHODOLOGY

To address the goals of this study, the following data were collected:

1. Forty-two measured sections totaling approximately 270 meters that document sedimentary structures, grain size and composition, and bedding surfaces at centimeter resolution (Figure 3.1).
2. Paleocurrent measurements ($n=3810$) collected from lineations, planes, barest surfaces, and channel margins. (Figure 3.2);
3. Gigapan photopanel were used to document story and bedset boundaries, facies locations, and thickness measurements of the paleochannel belt (Figure 3.3).
4. Morphometric characteristics of the channel belt including: width (w), thickness (t), sinuosity (s), radius of curvature (R_c), bend curvature (R_c/w), aspect ratio (w/t), and wavelength (λ) (Table 3.1).

These data were used to construct three cross-sections: a depositional-dip oriented cross-section on the north side of Segment 4, depositional-dip cross-section on the south side of Segment 4, and a deposition-strike-orientated cross-section on Segment 5 (Figure 3.1). The cross-sections document key stratal boundaries-the philosophical framework for identifying stratal boundaries is discussed below. Complimentary, annotated gigapan photopanel were used to document lithofacies, which in turn were used to calculate lithofacies proportions (Figure 3.1 and Appendix 2). Numbers in the cross-sections correlate to similar stories on each side of the channel belt. These numbers were assigned based on the data collected and available (Figure 3.1). The top of the channel belt is interpreted with a dashed line (Figure 3.1).

3.1 Fluvial Hierarchy

Bed, bedsets, and stories are recognized and documented in the studied outcrop. The fluvial hierarchy used in this study is based on Ford and Pyles (2014) (Figure 1.2), and is similar to Campbell (1967), and Van Wagoner et al (1990). A bed is defined as, “*a relatively conformable succession of genetically related laminae or lamina-sets bounded by surfaces (called bedding surfaces) of erosion, non-deposition, or their correlative conformities*” (Campbell, 1967, pg. 12). At this location, bed boundaries are usually amalgamated (sand-on-sand contact) due to erosion by successive beds (Figure 3.1). Occasionally, beds have topset preservation and its full foreset is preserved. Campbell (1967) defines bedset as, “*a relatively conformable succession of genetically related beds bounded by surfaces (called bedset surfaces) of erosion, non-deposition or their correlative conformities*” (Campbell, 1967, pg. 20). A bedset in the outcrop is bounded by erosional surfaces that are laterally persistent, and document abrupt grainsize differences. The base of a bedset is a coarser grained (upper to lower medium) than in top (lower medium to upper fine), meaning they have a fining upward profile within each bedset (Figure 3.1).

A story is “*a meso-scale volume of strata formed from genetically related beds or bedsets produced by the migration, fill or overbank discharge of a single fluvial system*” (Ford and Pyles, 2014, pg. 1281). In this field area, a story is recognized by superposition and cross-cutting relationships. Younger stories cross-cut and locally erode into an older and previously deposited story. Figure 3.1 depicts colored polygons, where each polygon represents an individual story. The cross-section

documents how younger stories cross-cut into the older stories. Individual stories also display components of both lateral accretion and downstream accretion.

Two types of stories are recognized: lateral and downstream (Lateral accretion dominated areas and downstream accretion dominated areas within stories were distinguished from one another by the strike and dip of the bedset surfaces. If a bedset surface has a strike that is parallel or subparallel ($\pm 20^\circ$) to the documented paleoflow (Figure 3.2), it was categorized as a lateral accretion surface, whereas if a bedset surface had a strike that is perpendicular or subperpendicular to paleoflow, that surface was categorized as a downstream accretion surface. Strike readings were plotted (Figure 3.2) and accretion type dominated areas could be separated from each other (Figure 3.1).

3.2 Lithofacies

This study uses Gressly's (1838) definition of lithofacies as, "*those observable physical, chemical and biological properties of rocks that collectively permit the objective description, as well as distinctions among rocks of different types*" (Translation from Cross and Homewood, 1997, pg. 1620). Three lithofacies were identified in this study. Each lithofacies is distinguished by grain-size and sedimentary structures. Descriptions and photographic examples are presented in Table 3.2 and Figure 3.4, respectively, and an example of an annotated cross-section is shown in Figure 3.3. Other examples are included in Appendix 2.

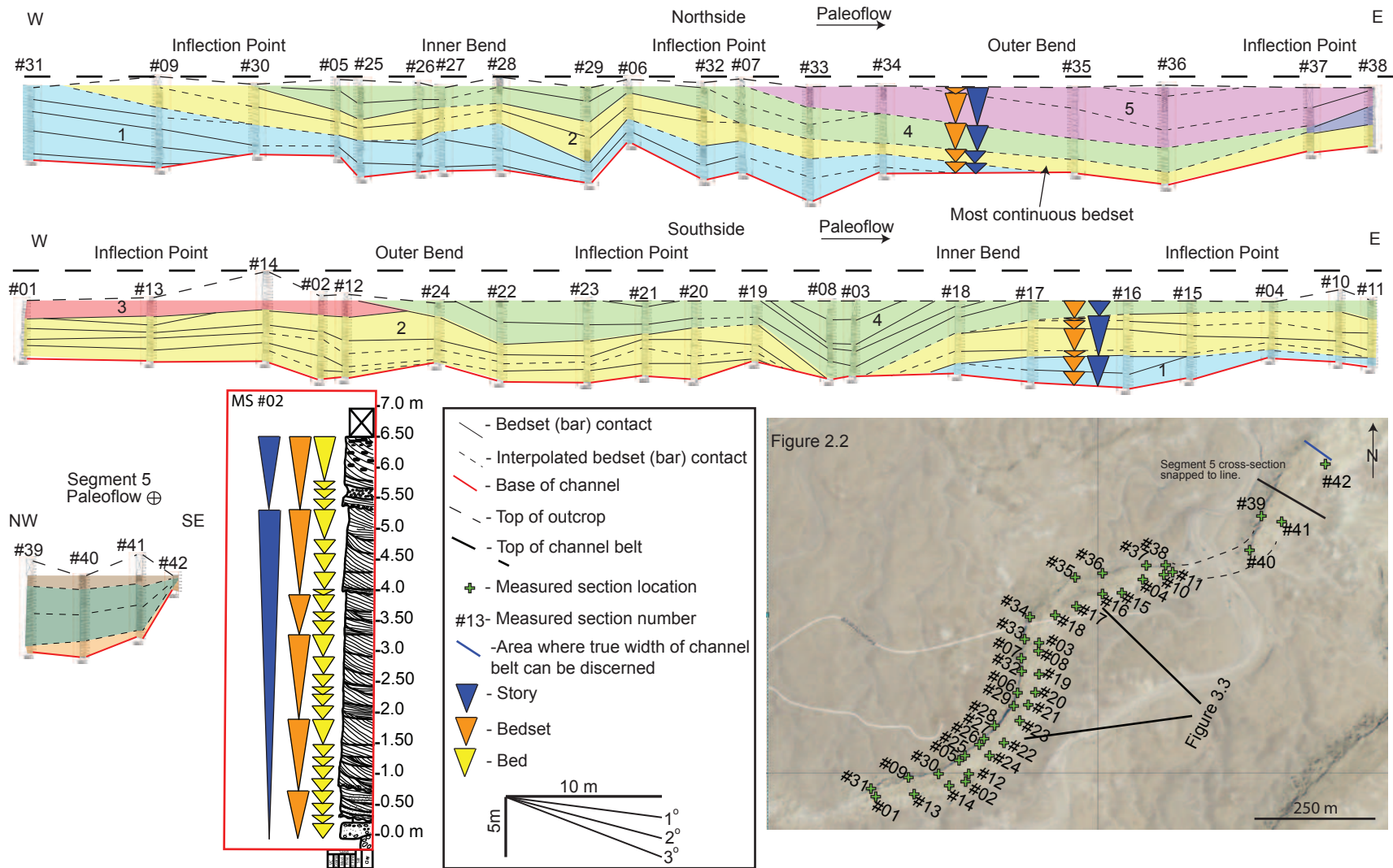


Figure 3.1: Dip-oriented cross-sections of the northern and southern sides of Channel Belt A, Segment 4, and a strike oriented cross-section of Segment 5. Location shown in Figure 2.1. See Appendix A for a detailed version of this image and larger versions of each measured section. Each color in the cross-sections is one individual story. Numbers in the cross-sections correspond to similar stories on each side of the channel belt.

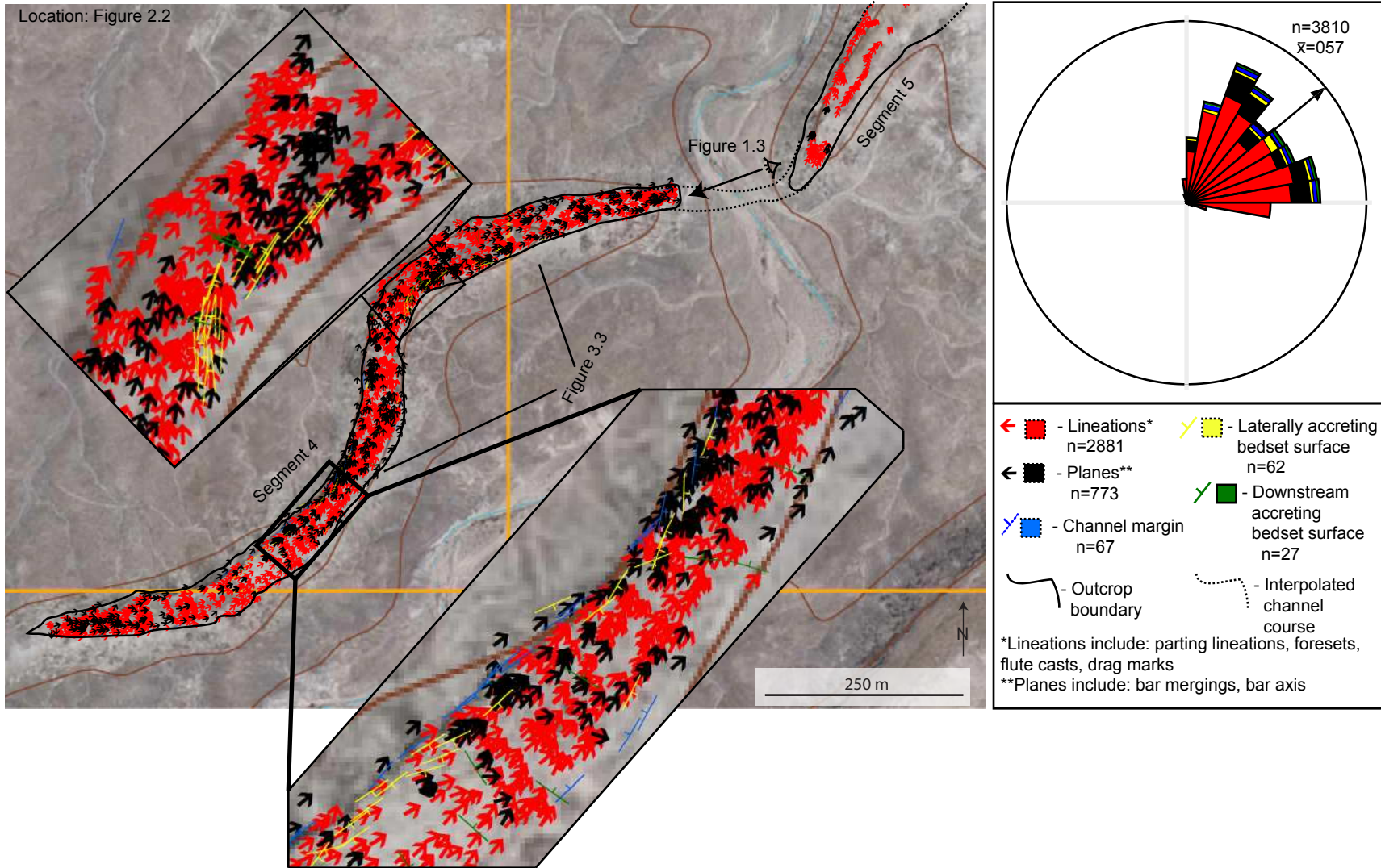


Figure 3.2: Satellite image of the study area. Segments 4 and 5 of Channel Belt A are the main focus of this study. The locations of collected paleocurrents are plotted on top of each segment. A total of 3,810 paleocurrents were collected from different sources (listed in key) and yielded an average paleocurrent direction of 057.

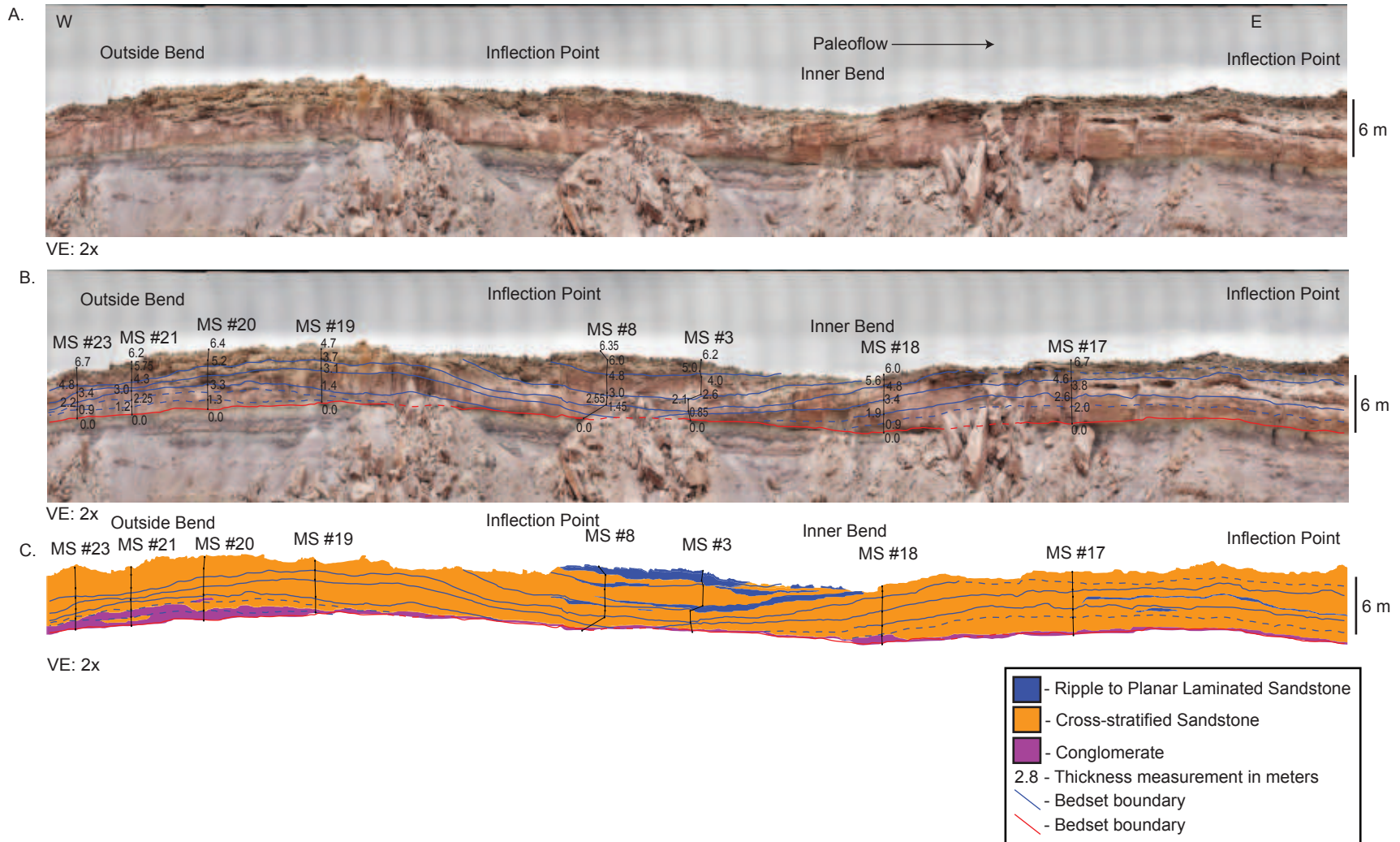


Figure 3.3: Representative photopanel from the central part of the study area. A) Uninterpreted photopanel. B) Photopanel with bedset (bar) contacts and locations of thickness measurements when gathering measured sections. C) Facies polygons used for lithofacies proportion analysis, and the same thickness measurements as B. See Figure 3.2 for location of photopanel. (See Appendix B for a complete series of panels around the studied segment)



Figure 3.4: Photographic examples of the 3 lithofacies of the studied interval. Descriptions and interpretations are summarized in Table 3.2.

Table 3.1: Morphometric characteristics of Channel A Segment 4 based on measurements taken from Google Earth.

Width (w)	80 meters
Average thickness	6.3 meters
Sinuosity (s)	1.2
Radius of curvature: Right bend (R_c)	175 meters
Radius of curvature: Left bend (R_c)	220 meters
Bend curvature (R_c/w): Right bend	2.2
Bend curvature (R_c/w): Left bend	2.8
Aspect ratio (w/t)	12.7
Wavelength (λ)	845 meters

Sinuosity=Channel meander distance divided by horizontal distance

Table 3.2: Descriptions of the 3 lithofacies identified in this study. See Figure 3.4 for photographic examples.

Color in Facies Polygons	Facies Name	Grain Size	Description	Interpretation
	Conglomerate	Upper Medium to Lower Coarse	Poorly sorted conglomerate containing paleosol and quartzite clasts up to 10 cm and 3 cm, respectively. Unstructured to cross-stratified bedding that terminates into underlying paleosol. Sharp to gradational upper contact, and sharp lower contact.	Lower flow-regime; tractive deposition; very high energy
	Cross-stratified sandstone	Lower Medium to Lower Coarse	Large-scale trough-cross bedding containing laminations that dip between 2° and 30° and range in thickness between 0.5 cm to 3 cm. Commonly contains rip-up clasts from adjacent mudstone. Slight upward-fining sequences that go from lower coarse sand to upper medium, or upper medium to lower medium sands. Reactivation surfaces are rarely observed. This lithofacies is often burrowed when it occurs at the top of the channel belt. Both sharp to gradational upper and lower contacts with other facies.	Lower flow-regime; tractive deposition; high energy
	Ripple-to-planar Laminated Sandstone	Upper Fine to Upper Medium	Ripple-to-planar laminated sandstone with laminations ranging from 0.1 to 1 cm. Rippled sandstone dominantly composed of upper fine to, rarely, lower medium. Planar-laminated sandstone is composed of lower medium to upper medium. Undulose laterally. Can be burrowed or bioturbated. Climbing ripples present, but rare. Gradational-to-sharp upper and lower contacts.	Lower flow-regime; tractive deposition; low energy

CHAPTER 4

RESULTS

The cross-sections and maps (Figure 4.1 and 4.2) document the facies distributions and paleo-geomorphology of the studied segment of Channel Belt A (Figure 2.2A). Each of these are discussed below.

Segments 4 and 5 of Channel A are exceptional exposures that document a complete wavelength of sinuosity (850 m) of an ancient channel belt. Two bends were documented, and associated straight portions (inflection points) of the channel belt were documented (Figure 1.3). Key geomorphic measures of the channel belt are the following (Table 3.1). The studied segment has a sinuosity (s) of 1.2. The radius of curvatures (r) of the left bend is 220 m and the right bend is 175 m. A width (w) of 80 meters was documented at a point where there is complete preservation of the channel's margins (at Segment 5, Figure 1.3). The average thickness (t) is 6.3 meters, leading to an aspect ratio (w/t) of 12.7.

Figure 4.1 documents lithofacies distributions in the studied channel belt by position: i.e. bends vs inflections. The dominant lithofacies in the channel belt is cross-stratified sandstone (83.5%). The second most common lithofacies is conglomerate (11.4%), followed by ripple-to-planar laminated sandstone (5.1%). Lithofacies relationships change by their geomorphic positions (i.e. outside bends, inside bends, and inflection points) and stratigraphic position in the channel belt (Figure 4.1). Outer bends contain all lithofacies, but are dominated by cross-stratified sandstone. For example the left bend contains cross-stratified sandstone (91.2%), conglomerate (8.1%), and ripple-to-planar laminated sandstone (0.7%). Whereas the right bend

contains cross-stratified sandstone (90.2%), conglomerate (8.7%), and ripple-to-planar laminated sandstone (1.1%) (Figure 4.1). Inner bends contain the highest abundance of ripple-to-planar laminated sandstone facies. For example the left bend contains cross-stratified sandstone (65.1%), conglomerate (8.8%), and ripple-to-planar laminated sandstone (26.1%), whereas the right bend contains cross-stratified sandstone (87.7%), conglomerate (5.0%), and ripple-to-planar laminated sandstone (7.4%) (Figure 4.1). Ripple-to-planar laminated sandstone lithofacies decrease downstream from inside bends (Inflection point 2: 24.2%, Inflection point 3: 2.9%). The inflection points located downstream from outside bends lack ripple-to-planar laminated sandstone facies. For example, Inflection point 2 contains cross-stratified sandstone (85.3%), and conglomerate (14.7%), and is lacking ripple-to-planar laminated sandstone (Figure 4.1). The same is true for Inflection point 3, and it contains cross-stratified sandstone (77.1%), conglomerate (22.9%), and is lacking ripple-to-planar laminated sandstone (Figure 4.1).

The sandstone in this channel belt is continuous across the entire channel belt. No mud drapes or mud plugs are documented in the studied channel segments. The only mud units within the channel belt are intra-formational rip-up clasts within the conglomerate. While sandstone is fully continuous, bedsets and stories are not (Figure 3.1). The most continuous bedset is 95% the wavelength of the outcrop. The most continuous stories on each side of the outcrop do not persist the entire wavelength.

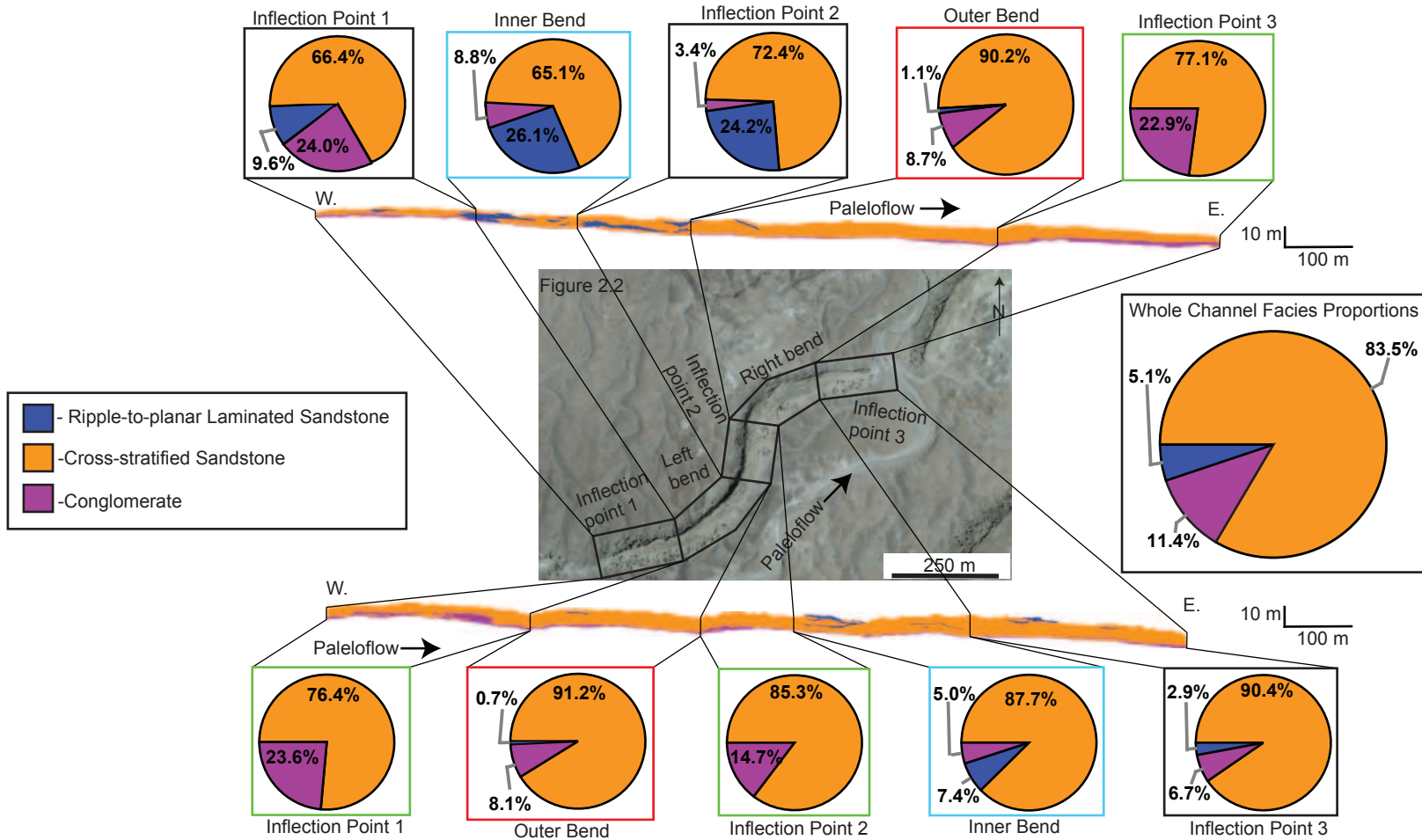


Figure 4.1: Map, cross sections, and pie charts documenting lithofacies proportions by geomorphic positions in the channel belt: outer bends, inner bends, and inflections points. Squares with similar colors represent corresponding geomorphic positions. This channel belt segment is largely dominated by cross-stratified sandstone. Outer bends contain comparable lithofacies proportions to each other. The same applies to inner bends and inflection points (straight segments of the channel belt). Outer bends contain all lithofacies, but are dominated by cross-stratified sandstone and inner bends contain the large proportions of ripple-to-planar laminated facies.

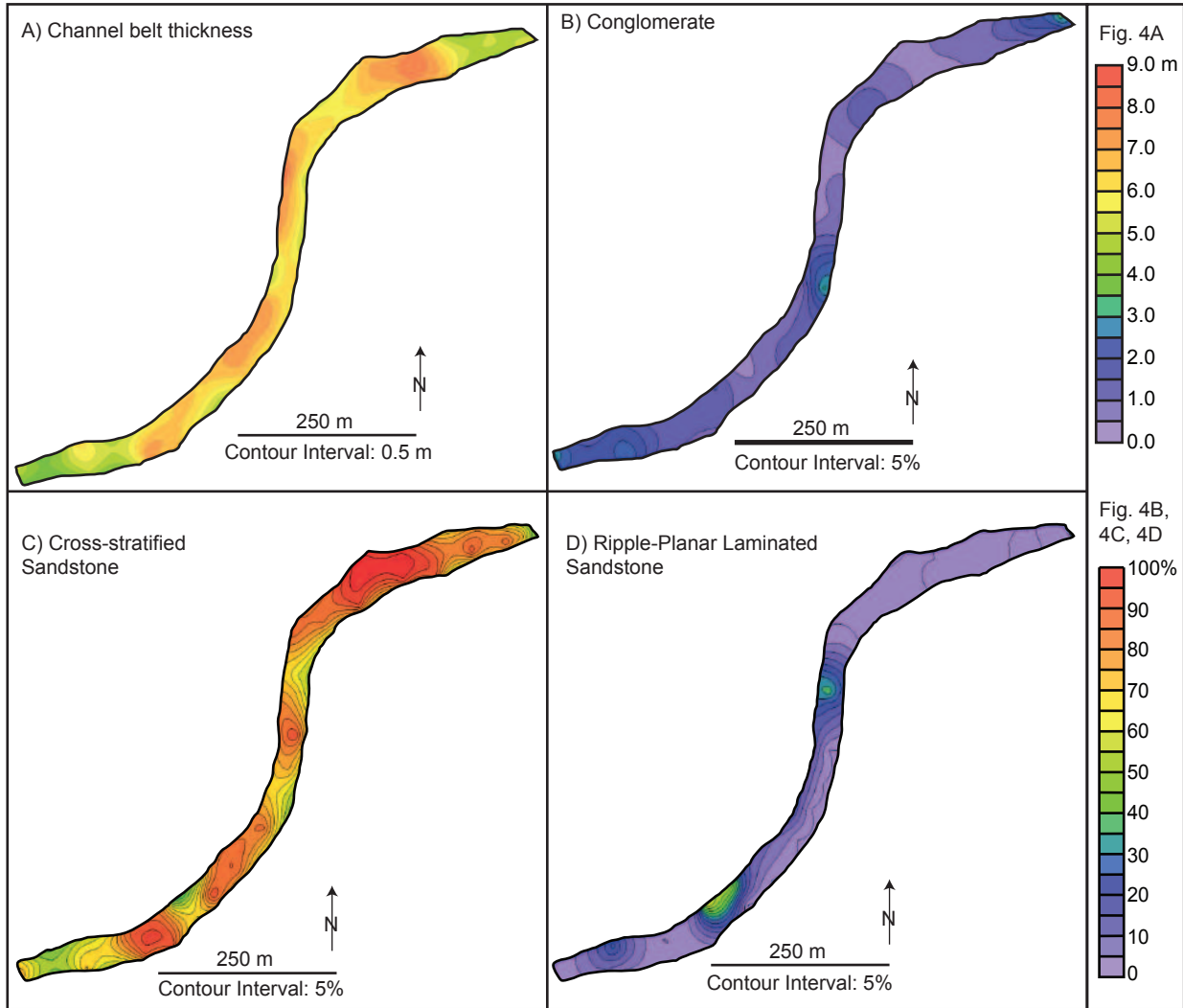


Figure 4.2: A) Isopach map of the studied segment of the channel belt. B) Percent thickness contour map of the conglomerate lithofacies. Conglomerate is present throughout the entire channel belt, but the thickest concentrations are located in the straight reaches (inflection points) of the channel belt. C) Percent thickness contour map of the cross-stratified sandstone lithofacies. This is the most prevalent lithofacies and its thickest areas are where the conglomerate is thinnest. D) Percent thickness contour map of the ripple-to-planar laminated sandstone lithofacies. This lithofacies has very localized concentrations in bends. Each lithofacies contour map is depicted at the same scale. Refer to Figure 2.2 for location.

CHAPTER 5

DISCUSSION

5.1 Continuity and Applications

Using photopanel and measured sections the longitudinal persistence of sandstone, bedsets, and stories were documented in the field. Sandstone within the outcrop is longitudinally persistent through the entire wavelength (Figures 3.1, 4.1, 4.2). While the channel belt is completely filled with sand, it still has grain-size variations and abrupt juxtapositions of grain sizes, although there is a lack of fine-grained sediment (i.e. clay and silt). These patterns are evident in the distribution of lithofacies (Figures 4.1 and 4.2) and are documented in detailed stratigraphic columns (Figure 3.1 and Appendix 1). The lack of fines is possibly due to perennial flow conditions, meaning there was a constant flow of fluids through the channel, leading to constant entrainment of clay and silt during the life span of the channel belt.

While sandstone is continuous across the entire interval, bedsets and stories are not. Figure 3.1 depicts cross-sections that document the bedset contacts for both sides of the outcrop. Younger bedsets cross-cut and erode into the previously deposited, older bedsets. Because of this erosion, the most longitudinally persistent bedset is 95% of the outcrop wavelength (Figure 3.1). Stories are also persistent for only a portion of the outcrop's wavelength. The most continuous story is colored in yellow on the southside of the channel belt and is continuous for 95% of the channel belt.

The observations listed above provide enhanced context for fluvial studies, fluvial reservoir models and fluvial physical experiments. Donselaar and Overeem (2008) document a difference in sandstone continuity based on different channel-fill

styles (Figure 1.1). Finer-grained channel fills result in low sandstone continuity, whereas sandier fill results in high sandstone continuity. The studied segments of Channel Belt A in the Cedar Mountain Formation are most similar to the channel belt model that has a sand fill with highly continuous sandstone in which the channel belt is filled with both lateral and downstream accreting bars (Figure 1.1A). Observations documented herein can be used to constrain intra-channel belt sedimentary structures, facies and their spatial locations within reservoir models of this style of channel belt. Figures 4.1 and 4.2 are notable data sets that can be used to constrain the proportions of overall lithofacies, accretion type and proportions, and lithofacies by accretion type in distinct areas of a channel belt. Static fluvial reservoir models can be constructed with these proportions to better represent the internal heterogeneity documented in a natural system. This internal heterogeneity can be useful to characterize flow units and permeability zones.

Chilingar (1964) documented relationships between porosity, permeability, and grain-size: as grain-size increases, so do porosity and permeability. Masch and Denny (1966), and Slatt et al. (1993) also reported similar results in regards to permeability and grain-size distribution from natural systems. This concept has significance for storage capacity and permeability distributions in fluvial sandstone reservoirs. When combining the permeability and grain-size distributions with the results of this research, fluvial reservoir models can be constrained. Collectively the data can predict of permeability streaks or zones based on facies locations. For example, the conglomerate lithofacies has variable thickness of 10 cm in the bends to 150 cm in the inflection points, however it present (although in particularly small proportions) throughout the entire channel belt

(Figure 4.1). The conglomerate lithofacies has the largest grain-size of the three lithofacies observed (Table 3.2) and, therefore, can be approximated to have the highest permeability. McGuire et al. (1995), Le Heron et al. (2004), Shepherd (2009), and Gershenzon et al. (2014) state that many hydrocarbon reservoirs contain conglomerates, and conglomerates are the most permeable zones. Often these zones are referred to as “thief zones” and are preferential pathways for subsurface fluid flow. These zones can also lead to early breakthrough of water in reservoirs connected to an aquifer and those undergoing secondary recovery such a water injection to increase hydrocarbon sweep efficiency (Gershenzon et al., 2014). Water could preferentially flow to the high permeability area, compromising the sweep efficiency by producing hydrocarbons within the permeable area but bypassing the hydrocarbons in lower permeability, although volumetrically significant, areas (McQuire et al., 1995; Shepherd, 2009; Gershenzon et al., 2014). Additionally this research documents where the conglomerate occurs and its proportions in geomorphic location (Figure 4.1 and 4.2). The conglomerate lithofacies is documented to have the largest grain size of the three documented lithofacies. Based on the previous discussion, if this Channel Belt A was a sandstone reservoir the conglomerate could be a thief zone where fluids would preferentially flow, and bypass hydrocarbons being held in the cross-stratified sandstone and ripple-to-planar laminated sandstone portions of the reservoir. Therefore, fluvial reservoirs models can be updated with permeability proxies and locations based on lithofacies’ grain-size, geomorphic location, and proportions.

5.2 Sequential Evolution and Flow Processes

The sequential evolution of the channel belt was derived from cross-cutting relationships, superposition, and facies types. The evolution of the channel belt is interpreted as follows: 1) channel down cutting and bypass, 2) deposition of conglomerate, 3) lateral migration of the channel and fill by laterally migrating and downstream migrating bars, 4) channel stabilization and final fill by downstream migrating bars until complete avulsion (Figure 5.1). During the first phase (channel down cutting), the channel incised into the adjacent mudstone (see inset pictures in Figure 1.3) (Figure 5.1). There are at least three possible process explanations for this. First, Parker et al. (2011) documented that high energy flows can erode into cohesive mudstone. Second, Hajek and Edmonds (2014) interpret that during incision, channels associated with clay-rich overbank deposits indicate low sediment flux (Q_s). Third, Hajek and Edmonds (2014) link coarse-grained systems to steep gradients and high shear stress (τ) at low flow depths. Lynds et al. (2014) express shear stress (τ) as

$$\tau = \rho_f * g * d * s \quad (5.1)$$

where ρ_f is fluid density, g is gravitational acceleration, d is flow depth, and s is slope. All these interpretations are equally plausible.

The second phase of the channel's evolution was deposition of conglomerate. Conglomerate was deposited along the entire base of the channel (Figure 4.1 and 4.2B) as the channel began migrated laterally (Figure 5.1), although the thickness of conglomerate is greatest in the inflection points (Figure 4.2). The conglomerate is overlapped by laterally migrating and downstream migrating bars (Figure 5.1). The conglomerate is composed of intraformational and extraformational clasts with an upper

medium and lower coarse sand matrix. Parker et al. (2011) documented that cohesive floodplain material can be entrained in fluid flow due to erosion of the outer bank, and consequently the mudstone is carried downstream. The intraformational mudclasts in the conglomerate are similar to and are derived from the adjacent mudstone.

Extraformational clasts come from the Sevier Uplift and from the underlying Morrison Formation (Harris, 1980). Intraformational mudclasts and extraformational clasts have sizes up to 10 cm and 3 cm, respectively. We interpret the conglomerate to have deposited under high shear stress (τ) that was able to entrain both mud rip-up clasts and extraformational clasts and move them downstream, while also maintaining a sand suspended load (Dietrich et al., 1989; Lynds et al., 2014).

Phase three of channel evolution is a low energy manifestation of processes in Phase 2. Figure 4.2A documents the thickest portions of the channel belt are in the bends and thinner areas are in the straight reaches (inflection points). It is also documented that the thickest proportions of conglomerate are in the straight reaches (inflection points) and thickest proportions of cross-stratified sandstone are in the bends. This can be explained by a combination of Equation 5.1 and helical flow. Corney et al. (2006, pg. 249-250) state helical flow is created by an imbalance of the curvature-induced centrifugal acceleration of flow and an inwardly directed radial pressure gradient, which results from the super-elevation of the water surface at the outside bend. Helical flow creates a higher flow depth (d) on the outside bend, and therefore increases τ on the outside bend, and the opposite is true of the inside bend. Therefore, τ is high enough on the outside bend to erode into the mudstone so the channel can migrate laterally and deepen, while also depositing the smaller grain sizes (ripple-to-

planar laminated sandstone, Figure 4.2D) on the inside bends as laterally accreting and downstream migrating bars. It also means that when exiting the bends and the helical flow has decreased or is nonexistent the boundary shear stress (τ) is not high enough to transport large clasts and sands any longer, resulting in thicker portions of conglomerate in the straight reaches (inflection points) of the channel (Figure 4.2B). Fourth, downstream migrating bars are documented to downlap on to laterally migrating bars in bends and fill the remaining space in the straight reaches (inflection points) (Figure 5.1). As downstream migrating bars filled the remaining space in the channel, the flow depth (d) decreased, thus continually decreasing τ (equation 5.1). This continued until the channel was completely filled and fluid flow avulsed to a new location.

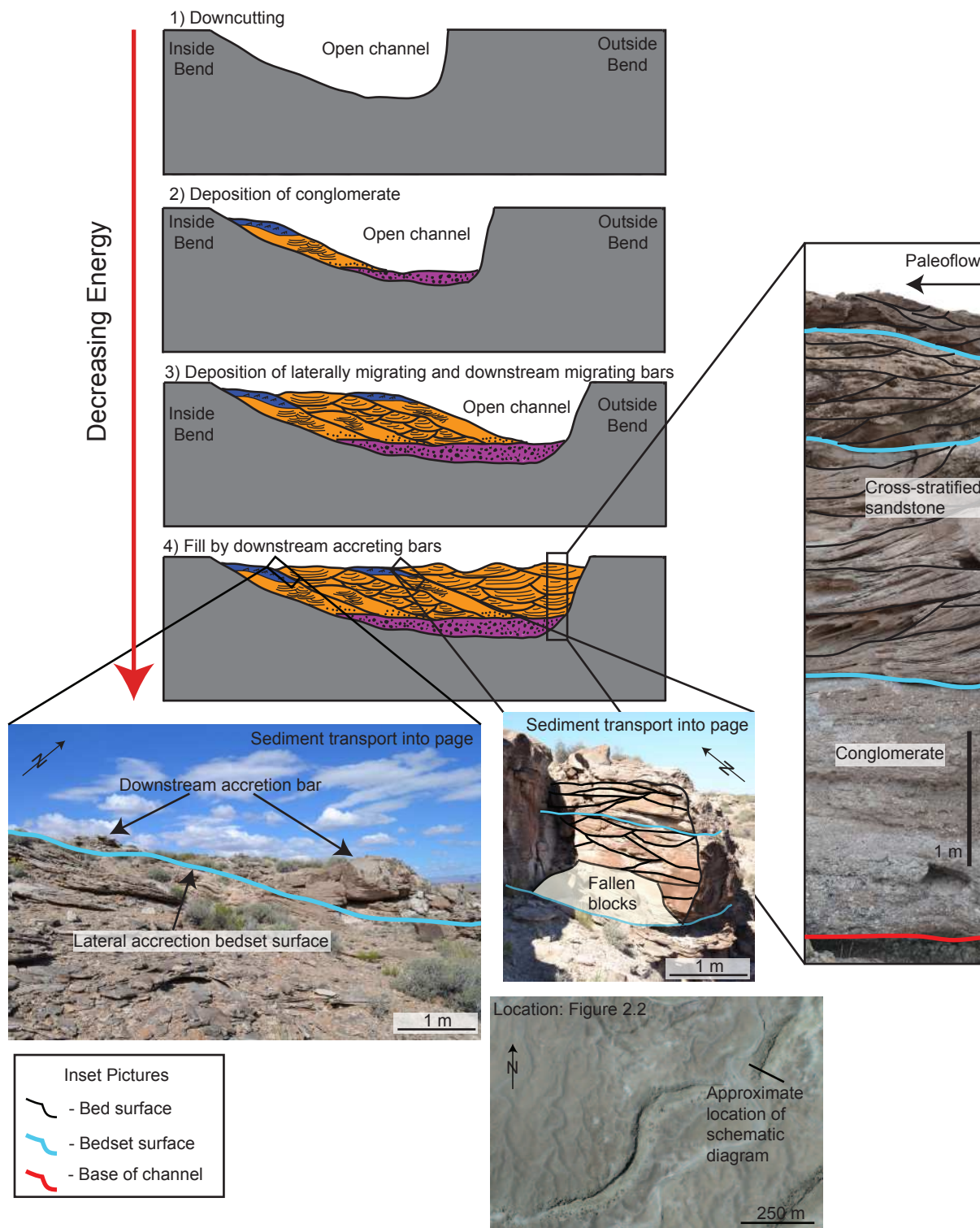


Figure 5.1: Schematic evolution the studied segments of Channel Belt A of the Cedar Mountain Formation: 1) Channel downcutting and bypass, 2) bypass and deposition of conglomerate, 3) lateral migration and fill by laterally migrating and downstream migrating bars. 4) Final fill by downstream migrating bars. Inset photographs are documented examples of surfaces and superposition seen at the outcrop.

CHAPTER 6

CONCLUSIONS

This thesis documents the lithofacies distributions by geomorphic location in a segment of one channel belt in the Cedar Mountain Formation. The studied channel belt is predominantly cross-stratified sandstone, with lesser amounts of conglomerate and ripple-to-planar laminated sandstone. Because this channel belt is filled with sand from both laterally accreting bars, and downstream accreting bars it is most similar to the sand channel fill model of Donseelar and Overeem (2008). Sandstone is continuous throughout the entire outcrop, however bedsets and stories are not. Based on cross-cutting relationships, superposition, and facies types the sequential evolution was interpreted along with the flow processes in each stage. Incision into the adjacent mudstone by high velocity fluids create a channel for fluid and sediment to be transported through. A conglomerate consisting of intraformational and extraformational clasts was continually deposited at the base of the channel as it began to laterally migrate. Finally, the channel stabilized and filled with both laterally migrating and downstream migrating bars simultaneously until it was completely filled and avulsed to a new location. Concepts developed here provide context for fluvial reservoir modelling and fluvial physical experiments.

REFERENCES CITED

- Aydin, A. (2000) Fractures, faults, and hydrocarbon entrapment, migration and flow. *Marine and Petroleum Geology*, 17, 797-814.
- Bridge, J. (2006) Fluvial facies models: recent developments. *SPECIAL PUBLICATION-SEPM*, 84, 85.
- Campbell, C.V. (1967) Lamina, laminaset, bed and bedset. *Sedimentology*, 8, 7-26.
- Chilingar, G.V. (1964) Relationship between porosity, permeability, and grain-size distribution of sands and sandstones. *Developments in Sedimentology*, 1, 71-75.
- Collinson, J. and Lewin, J. (1983) Modern and ancient fluvial systems: an introduction. In: *Modern and Ancient Fluvial Systems*, 6, pp. 1-2.
- Colombera, L., Felletti, F., Mountney, N.P. and McCaffrey, W.D. (2012a) A database approach for constraining stochastic simulations of the sedimentary heterogeneity of fluvial reservoirs. *AAPG bulletin*, 96, 2143-2166.
- Colombera, L., Mountney, N.P. and McCaffrey, W.D. (2012b) A relational database for the digitization of fluvial architecture concepts and example applications. *Petroleum Geoscience*, 18, 129-140.
- Corney, R.K., Peakall, J., Parsons, D.R., Elliott, L., Amos, K.J., Best, J.L., Keevil, G.M. and Ingham, D.B. (2006) The orientation of helical flow in curved channels. *Sedimentology*, 53, 249-257.
- Cross, T.A. and Homewood, P.W. (1997) Amanz Greesly's role in founding modern stratigraphy. *GSA Bulletin*, 109, 1617-1630.
- Currie, B.S. (1998) Upper Jurassic-Lower Cretaceous Morrison and Cedar Mountain Formations, Ne Utah-Nw Colorado: Relationships between Nonmarine Deposition and Early Cordilleran Foreland-Basin Development. *Journal of Sedimentary Research*, 68, 21.
- DeCelles, P. and Currie, B. (1996) Long-term sediment accumulation in the Middle Jurassic-early Eocene Cordilleran retroarc foreland-basin system. *Geology*, 24, 591-594.
- DeCelles, P.G. and Giles, K.A. (1996) Foreland basin systems. *Basin Research*, 8, 105-123.

- DeCelles, P.G., Lawton, T.F. and Mitra, G. (1995) Thrust timing, growth of structural culminations, and synorogenic sedimentation in the type Sevier orogenic belt, western United States. *Geology*, 23, 699-702.
- Derr, M.E. (1974) *Sedimentary structure and depositional environment of paleochannels in the Jurassic Morrison Formation near Green River, Utah*, Brigham Young University, Dept. of Geology., 42 pp.
- Dietrich, W.E., Kirchner, J.W., Ikeda, H. and Iseya, F. (1989) Sediment supply and the development of the coarse surface layer in gravel-bedded rivers. *Nature*, 340, 215-217.
- Donselaar, M.E. and Overeem, I. (2008) Connectivity of fluvial point-bar deposits: An example from the Miocene Huesca fluvial fan, Ebro Basin, Spain. *AAPG bulletin*, 92, 1109-1129.
- Doyle, J. and Sweet, M. (1995) Three-dimensional distribution of lithofacies, bounding surfaces, porosity, and permeability in a fluvial sandstone--Gypsy Sandstone of Northern Oklahoma. *AAPG bulletin*, 79, 70-95.
- Drinkwater, N. and Pickering, K. (2001) Architectural elements in a high-continuity sand-prone turbidite system, late Precambrian Kongsfjord Formation, northern Norway: Application to hydrocarbon reservoir characterization. *AAPG bulletin*, 85, 1731-1757.
- Fielding, C.R., Allen, J.P., Alexander, J. and Gibling, M.R. (2009) Facies model for fluvial systems in the seasonal tropics and subtropics. *Geology*, 37, 623-626.
- Ford, G.L. and Pyles, D.R. (2014) A hierarchical approach for evaluating fluvial systems: Architectural analysis and sequential evolution of the high net-sand content, middle Wasatch Formation, Uinta Basin, Utah. *AAPG Bulletin*, 98, 1273-1304.
- Galloway, W.E., Hobday, D.K. and Magara, K. (1982) Frio formation of the Texas Gulf Coast Basin-Depositional systems, structural framework, and hydrocarbon origin, migration, distribution, and exploration potential. *Rep. Invest., Univ. Tex. Austin, Bur. Econ. Geol.:(United States)*, 122.
- Gershenson, N.I., Soltanian, M., Ritzi, R.W. and Dominic, D.F. (2014) Understanding the impact of open-framework conglomerates on water–oil displacements: the Victor interval of the Ivishak Reservoir, Prudhoe Bay Field, Alaska. *Petroleum Geoscience*, 21, 12.
- Ghazi, S. and Mountney, N.P. (2009) Facies and architectural element analysis of a meandering fluvial succession: The Permian Warchha Sandstone, Salt Range, Pakistan. *Sedimentary Geology*, 221, 99-126.

- Gressly, A. (1838) Observations geologiques sur le Jura soleurois. *Nouveaux memoires de la Societe Helvetique des Sciences Naturelles, Neuchatel*, 2, 349.
- Hajek, E. and Edmonds, D. (2014) Is river avulsion style controlled by floodplain morphodynamics? *Geology*, 42, 199-202.
- Harris, D.R. (1980) *Exhumed paleochannels in the Lower Cretaceous Cedar Mountain Formation near Green River, Utah*, Brigham Young University, 16 pp.
- Kerr, D.R. and Jirik, L.A. (1990) Fluvial architecture and reservoir compartmentalization in the Oligocene middle Frio Formation, South Texas, 40, pp. 8. GCAGS.
- Kirkland, J.I. and Madsen, S.K. (2007) The Lower Cretaceous Cedar Mountain Formation, eastern Utah. In: *Field guide to geologic excursions in southern Utah, Geological Society of America, Rocky Mountain Section 2007 Annual Meeting, St. George, Utah. Utah Geological Association Publication*, 35, pp. 1-108.
- Kirkwood, S.G. (1976) *Stratigraphy and petroleum potential of the Cedar Mountain and Dakota Formations, northwestern Colorado*, Colorado School of Mines, 114 pp.
- Larue, D. and Friedmann, F. (2005) The controversy concerning stratigraphic architecture of channelized reservoirs and recovery by waterflooding. *Petroleum Geoscience*, 11, 131-146.
- Larue, D.K. and Hovadik, J. (2006) Connectivity of channelized reservoirs: a modelling approach. *Petroleum Geoscience*, 12, 291-308.
- Le Heron, D., Sutcliffe, O., Bourgig, K., Craig, J., Visentin, C. and Whittington, R. (2004) Sedimentary architecture of Upper Ordovician tunnel valleys, Gargaf Arch, Libya: implications for the genesis of a hydrocarbon reservoir. *GEOARABIA-MANAMA*, 9, 137-160.
- Lorenz, J.C., Cooper, S.P. and Olsson, W.A. (2006) Natural fracture distributions in sinuous, channel-fill sandstones of the Cedar Mountain Formation, Utah. *AAPG bulletin*, 90, 1293-1308.
- Lynds, R.M., Mohrig, D., Hajek, E.A. and Heller, P.L. (2014) Paleoslope Reconstruction In Sandy Suspended-Load-Dominant Rivers. *Journal of Sedimentary Research*, 84, 825-836.
- Masch, F.D. and Denny, K.J. (1966) Grain size distribution and its effect on the permeability of unconsolidated sands. *Water Resources Research*, 2, 665-677.
- McGuire, P., Spence, A., Stalkup, F. and Cooley, M. (1995) Core acquisition and analysis for optimization of the Prudhoe Bay miscible-gas project. *SPE reservoir engineering*, 10, 94-100.

- Miall, A.D. (2006) Reconstructing the architecture and sequence stratigraphy of the preserved fluvial record as a tool for reservoir development: A reality check. *AAPG bulletin*, 90, 989-1002.
- Miall, A.D. and Tyler, N. (1991) The three-dimensional facies architecture of terrigenous clastic sediments and its implications for hydrocarbon discovery and recovery. 309.
- Parker, G., Shimizu, Y., Wilkerson, G., Eke, E., Abad, J., Lauer, J., Paola, C., Dietrich, W. and Voller, V. (2011) A new framework for modeling the migration of meandering rivers. *Earth Surface Processes and Landforms*, 36, 70-86.
- Pranter, M.J., Ellison, A.I., Cole, R.D. and Patterson, P.E. (2007) Analysis and modeling of intermediate-scale reservoir heterogeneity based on a fluvial point-bar outcrop analog, Williams Fork Formation, Piceance Basin, Colorado. *AAPG bulletin*, 91, 1025-1051.
- Pranter, M.J., Vargas, M.F. and Davis, T.L. (2008) Characterization and 3D reservoir modelling of fluvial sandstones of the Williams Fork Formation, Rulison field, Piceance basin, Colorado, USA. *Journal of Geophysics and Engineering*, 5, 158.
- Qui, Y., Xue, P. and Xiao, J. (1987) Fluvial sandstone bodies as hydrocarbon reservoirs in lake basins. *SEPM*, 57, 14.
- Schumm, S. (1985) Patterns of alluvial rivers. *Annual Review of Earth and Planetary Sciences*, 13, 5.
- Shepherd, M. (2009) Braided Fluvial Reservoirs. *AAPG Memoir*, 91, 5.
- Slatt, R.M. (2006) *Stratigraphic reservoir characterization for petroleum geologists, geophysicists, and engineers*. Elsevier, 493 pp.
- Slatt, R.M., Phillips, S., Boak, J.M. and Lagoe, M.B. (1993) Scales of geologic heterogeneity of a deep-water sand giant oil field, Long Beach unit, Wilmington field, California. In: *Marine Clastic Reservoirs*, pp. 263-292. Springer.
- Stokes, W.L. (1944) Morrison Formation and related deposits in and adjacent to the Colorado Plateau. *Geological Society of America Bulletin*, 55, 951-992.
- Stokes, W.L. (1961) Fluvial and eolian sandstone bodies in Colorado Plateau. *AAPG Bulletin*, 28.
- Van Wagoner, J.C., Mitchum, R., Campion, K. and Rahmanian, V. (1990) Siliciclastic sequence stratigraphy in well logs, cores, and outcrops: concepts for high-resolution correlation of time and facies.

Williams, R.M., Chidsey Jr, T.C. and Eby, D.E. (2007) Exhumed paleochannels in central Utah—Analogues for raised curvilinear features on Mars. *Central Utah: diverse geology of a dynamic landscape*, 36, 221-235.

Williams, R.M., Irwin, R.P., Zimbelman, J.R., Chidsey, T.C. and Eby, D.E. (2011) Field guide to exhumed paleochannels near Green River, Utah: Terrestrial analogues for sinuous ridges on Mars. *Geological Society of America Special Papers*, 483, 483-505.

Young, R.G. (1960) Dakota Group of Colorado Plateau. *AAPG Bulletin*, 44, 156-194.

APPENDIX A

Measured Sections and Cross Sections—SUPPLEMENTAL ELECTRONIC MATERIAL

Appendix A comprises measured sections and cross sections of Channel Belt A, Segments 4 and 5 of the Cedar Mountain Formation.

Measured_Sections.PDF	Compiled document of measured sections that were documented in the study area.
Cross_Sections.PDF	Cross sections created from measured sections of Channel A, Segments 4 and 5. This is a larger version of Figure 3.1.

APPENDIX B

Outcrop Photopanel—SUPPLEMENTAL ELECTRONIC MATERIAL

Appendix B comprises uninterpreted and interpreted photopanel of the study area.

Photopanel.PDF	Uninterpreted and interpreted photopanel of the study area
Photopanel_Location.PDF	Shows the locations of where photopanel were taken and the outcrop they view